

# Nozzle configuration and in-cylinder pressure effects on fuel spray behaviour: studies using a rapid cycling machine

Darlington Njere and Nwabueze Emekwuru

**Author post-print (accepted) deposited by Coventry University's Repository**

**Original citation & hyperlink:**

Njere, D. and Emekwuru, N., 2021. Nozzle configuration and in-cylinder pressure effects on fuel spray behaviour: studies using a rapid cycling machine. *Journal of the Brazilian Society of Mechanical Sciences and Engineering*, 43(9), pp.1-20.

<https://doi.org/10.1007/s40430-021-03153-8>

DOI 10.1007/s40430-021-03153-8

ISSN 1678-5878

ESSN 1806-3691

Publisher: Springer

**The final publication is available at Springer via <https://doi.org/10.1007/s40430-021-03153-8>**

**Copyright © and Moral Rights are retained by the author(s) and/ or other copyright owners. A copy can be downloaded for personal non-commercial research or study, without prior permission or charge. This item cannot be reproduced or quoted extensively from without first obtaining permission in writing from the copyright holder(s). The content must not be changed in any way or sold commercially in any format or medium without the formal permission of the copyright holders.**

**This document is the author's post-print version, incorporating any revisions agreed during the peer-review process. Some differences between the published version and this version may remain and you are advised to consult the published version if you wish to cite from it.**

**Nozzle configuration and in-cylinder pressure effects on fuel spray behaviour: studies using a rapid cycling machine**

**Authors: Darlington Njere · Nwabueze Emekwuru**

**Journal of the Brazilian Society of Mechanical Sciences and Engineering**

“This version of the article has been accepted for publication, after peer review but is not the Version of Record and does not reflect post-acceptance improvements, proof work or any corrections. The Version of Record is available online at: <http://dx.doi.org/10.1007/s40430-021-03153-8> or from the SharedIt link at: <https://rdcu.be/cwoDP>.”

# NOZZLE CONFIGURATION AND IN-CYLINDER PRESSURE EFFECTS ON FUEL SPRAY BEHAVIOUR: STUDIES USING A RAPID CYCLING MACHINE.

Darlington Njere\*<sup>1</sup>, Nwabueze Emekwuru<sup>1, 2</sup>

<sup>1</sup>Faculty of Engineering, Environment and Computing,  
Coventry University, Coventry CV1 2JH, UK

<sup>2</sup>Transport Safety and Simulations Group, Institute for Future Transport and Cities,  
Coventry University, Coventry CV1 2TE, UK

## ABSTRACT

Efforts to improve the efficiency of internal combustion engines in applications such as heavy-duty vehicles where electric propulsion is currently unfeasible or need complementing are essential. However, studying the conditions of actual internal combustion engines while accessing their combustion chambers whilst they are in operation remains difficult. To allow for the characterisation of practical operating conditions of diesel engine designs, detailed studies examining the influence of the injector nozzle configuration, peak in-cylinder pressure conditions, and fuel injection pressure values up to 25 % greater than those hitherto typically reported using rapid cycling machines for diesel spray diagnosis were carried out. A rapid cycling machine using a production diesel engine piston design, equipped with optical windows and fitted with a high-pressure common rail fuel injection equipment was used with temporal spray liquid and vapour penetration values obtained using Schlieren and Mie scattering imaging techniques for injector nozzles of various  $k$ -factor values. Even though the effects of the different injector nozzle conicity values on the fuel spray liquid and vapour penetration values observed were not significant, the studies supported the use of such methods to evaluate the piston and cylinder wall wetting which can have significant effects on the emissions and fuel consumption from internal combustion engines. These are also useful for internal combustion engine design and numerical spray code development.

**Keywords:** Injection pressure, diesel, cavitation, optical engine,  $k/ks$ -factor, single cylinder research engine, rapid cycling machine, vapour penetration, liquid penetration, conicity, optical research, rapid compression machine.

## INTRODUCTION

The emissions “cycle beating” controversy [1] and the implementation of tougher emission standards (Table 1; [2]) have increased the already tough challenges the design of present and future diesel engines face. However, diesel engines, and indeed internal combustion engines, are still relevant for heavy duty vehicles, off highway vehicles, hybrid engines, electric generators, and in regions where electric vehicles might not be available for a while due to lack of infrastructure, hence their continued development is essential to reduce emissions due to their use. The combustion of diesel fuel in internal combustion engines may be influenced by the injector nozzle configuration that provides the atomization of the fuel [3]. Spray liquid and vapour penetration are considered important performance parameters in diesel engines as the optimum engine performance (low emissions, low fuel consumption) can be achieved if these are matched to the geometry and size of the diesel engine combustion chamber [3].

Ideally, researchers would like to study the influence of the injector nozzle configurations at the operating conditions encountered by actual diesel engines, but the difficulty of access to the combustion chamber whilst the engine is in operation has been a major constraint. Optically Accessed Research Engines (OAREs) are the test equipment most resembling actual diesel engines [4, 5]. The concept behind these is to modify various components of an actual diesel engine to allow optical access for spray and combustion studies [6].

Table 1: European Emissions standards for passenger vehicles, g/km [2]. Passenger vehicles are required to meet emission limits up to 91 % less than those from 20 years earlier.

Type of emission standard	Type approval date for vehicle	First Registration date for vehicle	CO	NO <sub>x</sub>	HC + NO <sub>x</sub>	PM	PN (#/km)
Diesel engine passenger vehicle							
Euro 3	January 2000	January 2001	0.66	0.50	0.56	0.0500	-
Euro 4	January 2005	January 2006	0.50	0.25	0.30	0.0250	-
Euro 5a	January 2009	January 2010	0.50	0.18	0.23	0.0050	-
Euro 6d	January 2020	January 2021	0.50	0.08	0.17	0.0045	6 x 10 <sup>11</sup>
Euro 6d standard difference relative to Euro 3 standard.			<b>-24%</b>	<b>-84%</b>	<b>-70%</b>	<b>-91%</b>	-
CO – Carbon Monoxide; NO <sub>x</sub> – Nitrogen Oxide; HC – Hydrocarbons; PM – Particulate Matter; PN – Particle Number							

However, these engines often require extensive, expensive modifications that also constrain the compression ratio values and the possible fuel spray penetration during operation [4]. A “purer” approach to studying diesel spray and combustion processes is to use Rapid Compression Engines; these systems are designed such that a piston completes one compression stroke before being brought to rest. They avoid the cycle to cycle variations and effects due to the complex nature of engine operating conditions [4, 7]. However, for the reliable interpretation of the data from these machines and to be able to use them to develop diesel fuel spray models reliably, the fluid mechanics, temperature, and pressure within the reaction chambers have to be properly characterized; this makes them complex and expensive [4, 7]. To allow for unconfined diesel fuel spray combustion and penetration studies many laboratories utilize the so-called combustion “bombs” [8], which could be either constant-volume test cells [4, 9, 10] or constant pressure test cells [4, 9, 10]. However, these test cells are, by their nature, less similar to actual engines in operation compared to the OAREs [4]. To offer some of the advantages of the combustion “bombs” to the OARE, purpose-built research engines are available, which use regular piston designs for diesel fuel engines (as does the OARE) but offer more combustion chamber space (thus more space for spray penetration studies) due to a further modified cylinder head. These so-called Rapid Cycling Machines [4, 11] can have their cylinder heads and other ancillaries changed or modified, and, thus can be adapted to future research needs. Table 2 presents a summary of these test equipment.

Table 2: Examples of test equipment used by researchers for evaluating diesel fuel spray characteristics. Adapted from [4, 5, 10].

Test equipment					
Type	Research engines with moving pistons			Combustion “bombs”	
Sub-type <sup>1</sup>	Optically Accessed Research Engine	Rapid Cycling Machine	Rapid Compression Machine	Constant-volume pre-burn chamber	Constant-pressure flow chamber
Details <sup>2</sup>	Production specification (possibly multi-cylinder) diesel engine modified to allow optical access to the combustion chamber.	Purpose built (single-cylinder) optically accessed research engine. Modifiable to accommodate future operating conditions.	Purpose built machine that allows a single compression stroke of the piston.	Pre-mixed combustion used to get the test section to the desired operating conditions before the diesel fuel is injected.	Ambient gases compressed and heated before the test section. Continuous gas flow in test section to maintain ambient temperature.
Similarity to actual diesel engine operating conditions <sup>3</sup>	5	4	4	2	2
Combustion space for diesel spray penetration <sup>3</sup>	1	3	3	5	5
Optical accessibility <sup>3</sup>	2	5	2	3	4
Modularity, adaptability for future operating conditions <sup>3</sup>	1	5	2	5	5

<sup>1</sup> The characterization or naming of the types of test equipment varies amongst researchers.

<sup>2</sup> These descriptions are the clearest differentiators the authors could use.

<sup>3</sup> Comparative assessments; 5 -most suitable, to 1 – least suitable, amongst 5 research test cells.

Scholars [4 – 11] have described diesel spray studies using the various types of test equipment.

The typical fuel injection pressure upper limit for production diesel systems has risen from about 1500 bar ten years ago to about 1000 bar more than that presently [12], with a range of 300 to 2400 bar [13]. Current research is tending towards greater than 3000 bar capable diesel fuel injection systems [12 - 15]. Several studies evaluating the influence of representative diesel engine in-cylinder operating conditions on the performance of diesel engines have been presented; most of them have been for diesel fuel spray combustion studies, with the results indicating reductions in the NO<sub>x</sub> emissions with increasing fuel injection pressure values, but with increases in soot emissions [15]. Visualization studies have shown the impact of the injector type on the cylinder wall-wetting [26], the effect of swirl flow pattern on combustion [24], and the use of EGR rate to control the NO<sub>x</sub> emissions at high injection pressure values [20]. Also, the impact of the injector nozzle configuration on the particle and soot emissions has been reported [15]. The reported operating conditions for these combustion studies range from 860 to 3300 bar for the maximum fuel injection pressure and in-cylinder pressure values of 11.5 to 300 bar [6, 15, 20, 26]. Comparatively fewer studies exist that evaluated the effect of in-cylinder conditions on the fuel liquid penetration [11, 16, 17]. At high fuel injection pressure values, the fuel vapour and spray penetration values increase but this trend is reversed with increasing in-cylinder pressure values [17]. Researchers studying diesel fuel spray penetration conditions using constant volume pressure vessels have reported injection pressure values of up to 3000 bar [13, 27, 28]. However, out of the test methods, these chambers least resemble actual engines (Table 2). In contrast, for rapid cycling machines, which more resemble actual engines (Table 2), only peak fuel injection values of up to 1600 bar and in-cylinder pressure value of 100 bar have been reported. Only one known study completely describes the effect of in-cylinder conditions *and* the fuel injector configurations on the fuel vapour *and* liquid penetration [17]. These are summarised in Table 3.

The work presented in this paper is concerned with the results from in-cylinder tests, carried out using a rapid cycling machine, that examined the influence of the injector nozzle configuration, peak in-cylinder pressure conditions, and fuel injection pressure values, 25 % higher than previously reported in literature, on diesel fuel spray liquid and vapour penetration, which is more representative of the present diesel engine operating conditions (Figure 1).

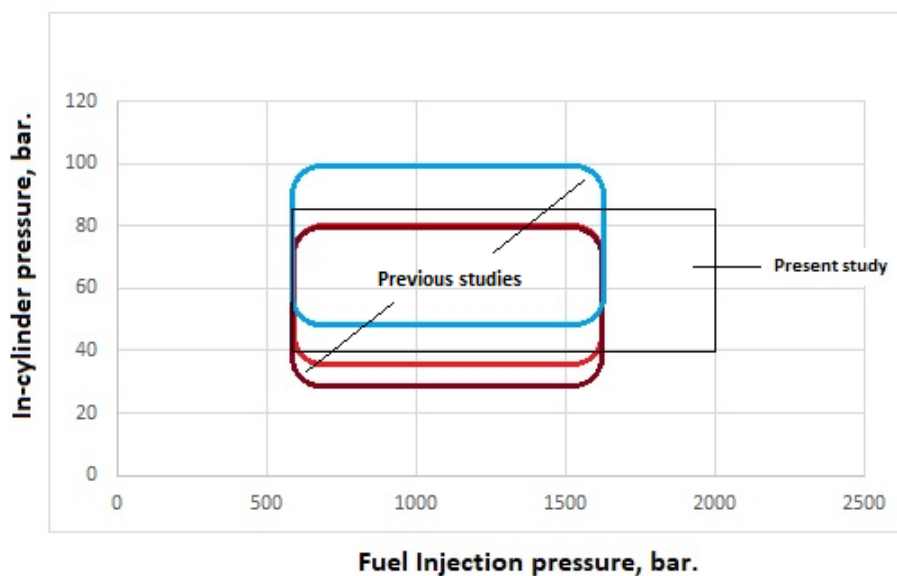


Figure 1: The present study presents results for the effects of in-cylinder conditions and fuel injector configurations on the fuel vapour and liquid penetration values, at presently representative operating conditions. Previous studies: — [11]; — [16]; — [17].

Table 3: Summary of literature on single cylinder diesel spray research studies.

Reference	Reported test conditions: peak values.	Consideration of: [i]. Diesel in-cylinder pressure conditions. [ii] Diesel injection pressure conditions. [iii] Diesel injector nozzle configurations; As they affect: [iv] Diesel fuel spray liquid penetration. [v] Diesel fuel spray vapour penetration.	Notes. Results.
Kennaird et al. [11]. 2000	In-cylinder pressure: 80 bar. Injection pressure: 1600 bar. Injector nozzle type: VCO.	Yes – [i] [ii] [iv]. No – [iii] [v].	Achieved in-cylinder pressure of 80 bar, compared to 60 bar maximum achievable at the time.
Morgan et al [16]. 2001	In-cylinder pressure: 80 bar. Injection pressure: 1600 bar. Injector nozzle types: VCO and mini-sac.	Yes – [i] [ii] [iii] [iv] [v].	Lucas single hole nozzles. Vaporizing and non-vaporizing conditions.
Laguitton et al. [17]. 2002	In-cylinder pressure: 100 bar. Injection pressure: 1600 bar. Injector nozzle type: VCO and mini-sac.	Yes – [i] [ii] [iii] [iv] [v].	The effects of the injector nozzle configurations were only presented for ignition delay values.
Lacoste et. [18]. 2003	In-cylinder pressure: 60 bar. Injection pressure: 1600 bar. Injector nozzle type: VCO.	Yes – [i] [ii]. No – [iii] [iv] [v].	Bosch common-rail. Single – hole. Droplet size and velocity studies.
Mueller et al. [25]. 2004	In-cylinder pressure: Injection pressure: 1420 bar. Injector nozzle type: VCO.	Spray visualization. Dual-injection cases. Heat-release analysis	Optical Research engine based on 1-cyl. Caterpillar C-10. Caterpillar HEUI injector.
Wloka et al. [15]. 2010	In-cylinder pressure: 300 bar. Injection pressure: 3200 bar. Injector nozzle type: VCO.	Injector nozzle configuration Particle and soot emissions.	No spray penetration. Single cylinder engine. Figures missing

Fuyuto et al. [26]. 2011	In-cylinder pressure: 11.5 bar. Injection pressure: 1800 bar. Injector nozzle type: VCO.	Spray visualization. Combustion images. Wall-wetting studies	Window cleaning mechanism
Zegers et al [19]. 2012	In-cylinder pressure: 60 bar. Injection pressure: 2500 bar.	Yes – [i] [ii]. No – [iii] [iv] [v].	Delphi Diesel Systems injector. Droplet velocity and velocity field studies.
Wickman, et al. [21] 2000	Injection pressure: 2600 bar.	NO <sub>x</sub> studies.	Caterpillar SCOTE 1 cylinder - engine
Musculus [23]. 2006	Injection pressure: 1600 bar	Fuel vapour penetration. Combustion.	Sandia Cummins N 1-cylinder engine
Dembinski [24]. 2014	In-cylinder pressure: Injection pressure: 2500 bar. Injector nozzle type: sac.	Swirl, flow pattern, combustion	Lotus AVT system. 1-cylinder engine
Morgan et al. [20]. 2015	In-cylinder pressure: 22.5 bar. Injection pressure: 3300 bar. Injector nozzle type: VCO.	NO <sub>x</sub> emissions using EGR rate.	Delphi f2E fuel injector. Controlling
Palanisamy et [12]. 2015	Injection pressure: 3000 bar.	Heat release, swirl, soot, NO <sub>x</sub>	AVL 1-cylinder research engine
Espec & Dec [6]. 1993	In-cylinder pressure: 60 bar. Injection pressure: 860 bar.	No. Combustion studies	Cummins 8 hole closed-nozzle injector. Combustion studies (soot).
Johnson, et al. [13]. 2013	In-cylinder pressure: density. Injection pressure: 3000 bar. Injector nozzle type: sac.	Injection pressure. Liquid penetration	Constant volume chamber
Jia et al [27]. 2017	Injection pressure: 3000 bar.	Induced shock waves	Constant volume chamber
Nishida et al [28].2017	Injection pressure: 3000 bar.	Liquid penetration	Constant volume chamber
Arcoumanis et al. [22].1994	Load: 10 bar	Spray penetration. Combustion.	4-cylinder optical VW engine. Fuel injection values not presented.

The next section of the paper describes the methodology used for the tests. The results from the tests are then presented and analysed. The implications of these for diesel and internal combustion engine development are then finally presented.

## METHODOLOGY

Experiments were carried using optical techniques to visualize in-cylinder characteristics in a rapid cycling engine.

### The Proteus Engine

The Proteus Engine is a 2-stroke, liner ported, single cylinder reciprocating rapid cycling machine. Specifications of the Proteus rig are: 150 mm stroke, 135 mm bore, 275 mm con-rod length and 2200 cc displacement and 9:1 compression ratio (Figure 2). Its single cylinder design permits spray visualisation under a wide range of operating conditions and easy access of optical diagnostics with minimized amount of test fuel.

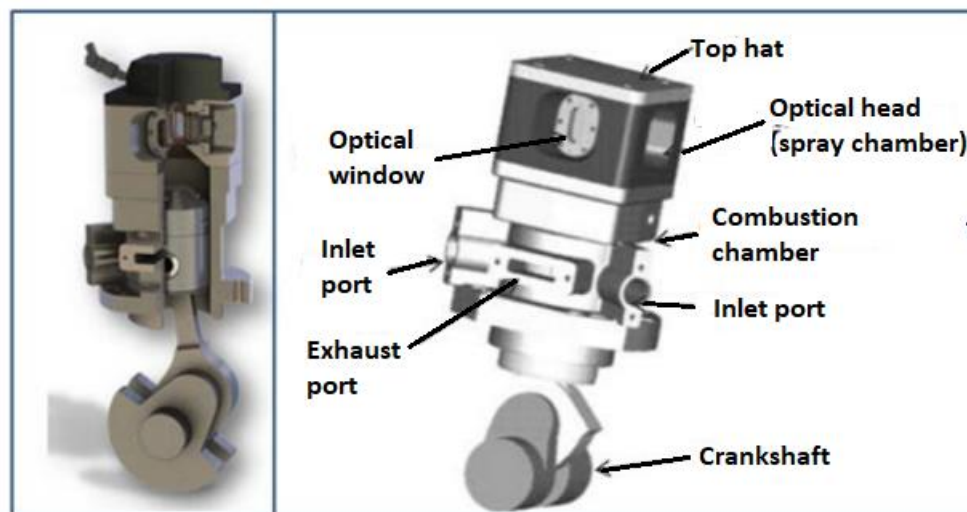


Figure 2: A Computer Aided Design rendering of the Proteus engine (left). Details of the Proteus engine showing the specially designed head with a top-hat shape and optical chamber, accessed by four removable windows (right). [29]

Due to the increased volume of the combustion chamber, the compression ratio (CR) was reduced to achieve optical access. As the compression ratio is a key element in reproducing similar conditions with production engines, it was therefore necessary to condition the intake air to be representative of production engines. The reduced CR also brings some measure of control as early auto-ignition of the fuel/air mixture is avoided. As optical access entails a less-efficient cooling system of the optical combustion chamber compared to a production engine, the Proteus Engine operates skip-fire modes to help reduce the thermal load on the engine, avoid unnecessary window fouling, maximise in-cylinder purging and ensure proper laser synchronisation. The Proteus engine was optimised using the Ricardo WAVE<sup>®</sup> and VECTIS<sup>®</sup> CFD codes for the ports, piston and air motion to achieve efficient scavenging and near quiescent air in the optical chamber using techniques presented in [30]. Disturbances due to air motion against spray development, especially at the top dead centre (TDC), are, therefore, reduced with good scavenging efficiency.

The Proteus engine was coupled to a DC dynamometer (3,000 rpm) via a reduction gearbox ratio of 6:1, corresponding to an engine operating speed of 500 rpm. Before initiating motoring operations, the water jacket and the sump oil were heated with immersion heaters to 85 °C and 35 °C respectively and delivered (via water and oil pumps) to heat the cylinder head, thus, minimising losses due to heat transfer from the in-cylinder gas to the surrounding walls. The rig was instrumented with appropriate sensors for condition monitoring with the details presented on Table 4.

Table 4: Sensors for condition monitoring used in the Proteus engine.

Sensor	Model	Where used	Range [bar]	Uncertainty [% full-scale output (FSO)]
Kistler	4045A		0 to 500	$\leq \pm 0.3$
Kistler	4067	Injector rail and delivery pipe pressure	0 to 5000	$\leq \pm 0.5$
Kistler	6155BU20	In-cylinder pressure	0 to 250	$\leq \pm 0.5$

### The Fuel Injection System

A high pressure (HP) common-rail system (CRS) fuel injection equipment, capable of achieving injection pressures up to 2000 bar, was used for the present study (**Error! Reference source not found.**). An external electric motor was used to run the CRS pump independent of the engine. The fuel was pressurized to the pre-set rail pressure before the appropriate quantity of fuel was transferred to the rail, ensuring a stable line pressure with minimum fluctuation.

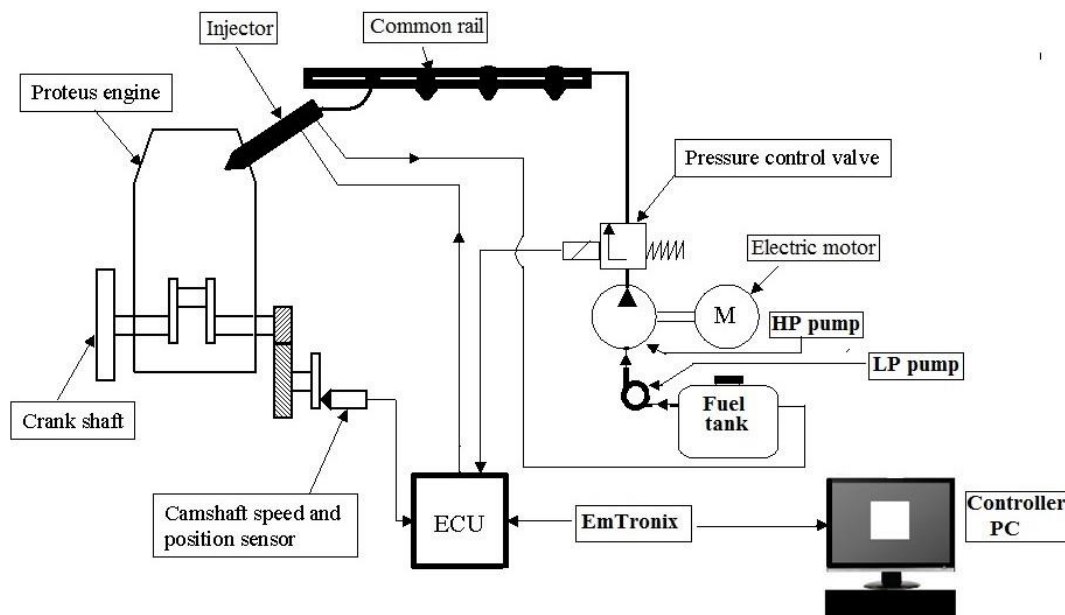


Figure 3: A schematic view of the fuel injection system used for the experiments [29].

Four different injectors were used for the tests (Figure 4; Table 5).



Figure 4: Eight-hole Delphi DFI 1.5 fuel injector used for the tests. [29]

Table 5: Specifications for the fuel injectors

Injector	Model	Number of Holes	Hole diameter (mm)	Flow rate (cc/min)	Cone angle (°)	<i>k</i> -factor
A	Delphi DFI 1.5	7	0.131	770	155	2.0
B	Delphi DFI 1.5	8	0.130	860	156	1.5
C	Bosch 3601 customised	8	0.137	960	155	1.3
D	Bosch 3603 customised	8	0.137	960	155	3.5

The injectors are classified by the *k*-factor parameter defined in equation (1) below [31]:

$$k = \frac{(D_{inlet} - D_{outlet})}{10} \quad (1)$$

Where *k* is the *k*-factor, a measure of conicity;  $D_{inlet}$  and  $D_{outlet}$  are the inlet and outlet orifice diameters in micrometres ( $\mu\text{m}$ ), respectively.

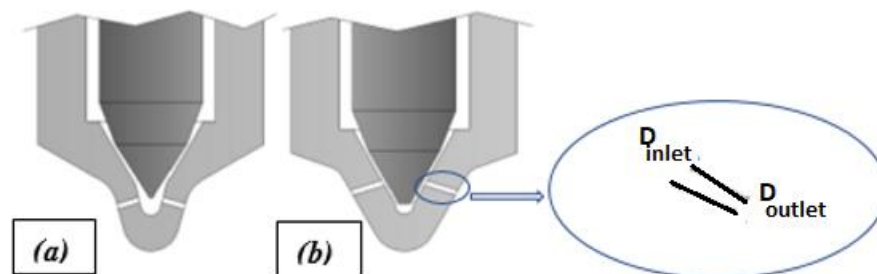


Figure 5: Schematic of injector nozzle types, (a) Sac, and (b) VCO, showing the characterisation of the inlet and outlet diameters, as used for the definition of the *k*-factor. Adapted from [32].

The  $k$ -factor describes the nozzle hole in terms of the diameter difference between the inlet and outlet of the nozzle hole (Figure 5).

Injectors C and D (Table 5) have the same hole diameters but different  $k$ -factors, the later having a different nozzle hole entrance geometry, obtained by a specifically designed hydro-grading process, of the type designated as  $ks$ -hole (see Figure. 6c), designed to improve spray stability. Only one, out of the four common rail injector outlets, was used at any given time, so the other unused three were fitted with plugs. For the rig, a special microprocessor-based controller implemented by an EmTronix system enabled independent control of the injection timing, number of injections per cycle, injection duration and rail pressure. A copper-vapour laser (CVL) strobe (Figures 7 and 8) was operated at 50,000 Hz pulsing frequency to illuminate the in-cylinder spray through the optical window. CMOS-based high-speed cameras (Phantom v12.1 and v710) were used for the tests, and were operated in the 41,000 - 42,000 Hz framing speed range for exposure times of 23 - 24  $\mu$ s.

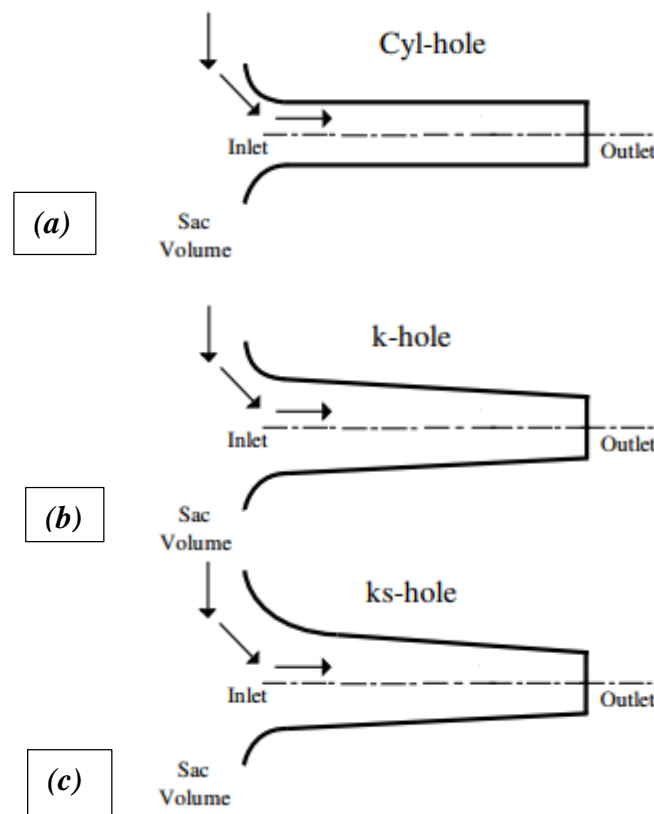


Figure 6: Schematic of different  $k$ -factor configurations: (a) cylindrical nozzle hole, (b) and (c) conical nozzle holes. Adapted from [33].

### Experimental techniques for the fuel spray characterization

Experiments were conducted to investigate liquid and vapour diesel fuel spray penetration values. A reference fuel (Carcal RF06-08-B5, density @ 15 °C of 0.833 g/mL) with low sulphur content and representative of automotive diesel was used for the experiments. Engine logs were recorded with the AVL Indiset high speed data acquisition system for fast logs (crank angle resolved), and EmTronics data logger for

slow logs. For each regime of test, a minimum of fifty (50) videos were acquired with the laser/camera combination. The videos were post-processed with a MATLAB<sup>®</sup> based in-house software and analysed.

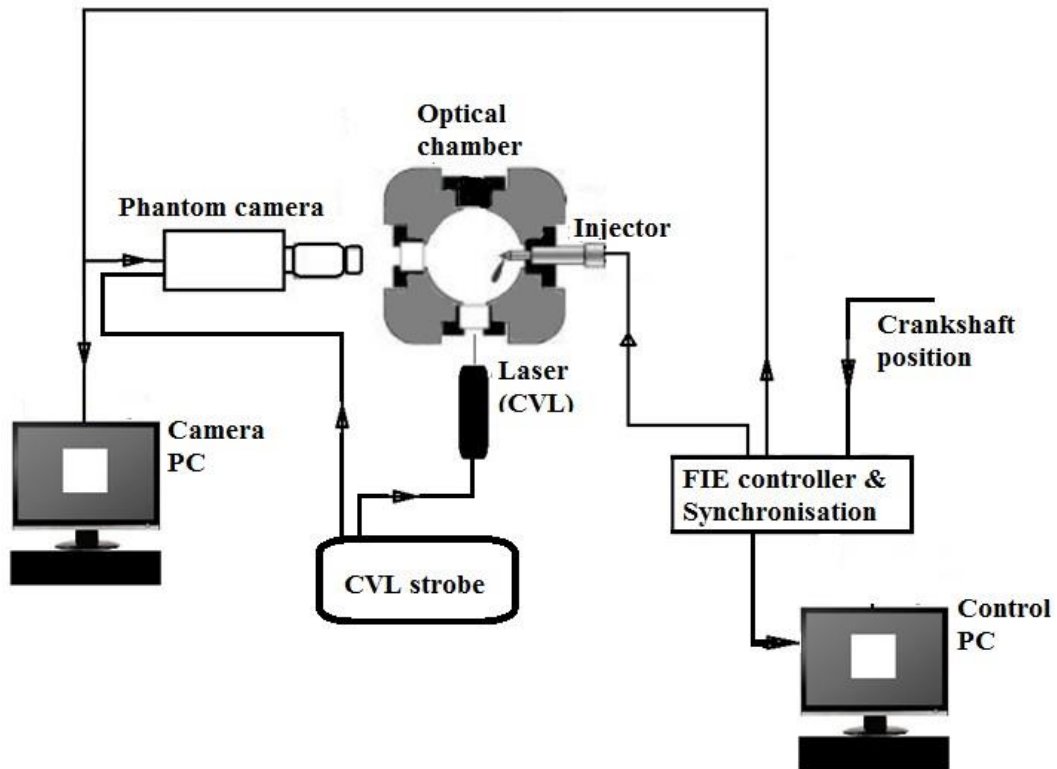


Figure 7: The schematic for the experimental set-up for the liquid spray visualization. [34, 35]

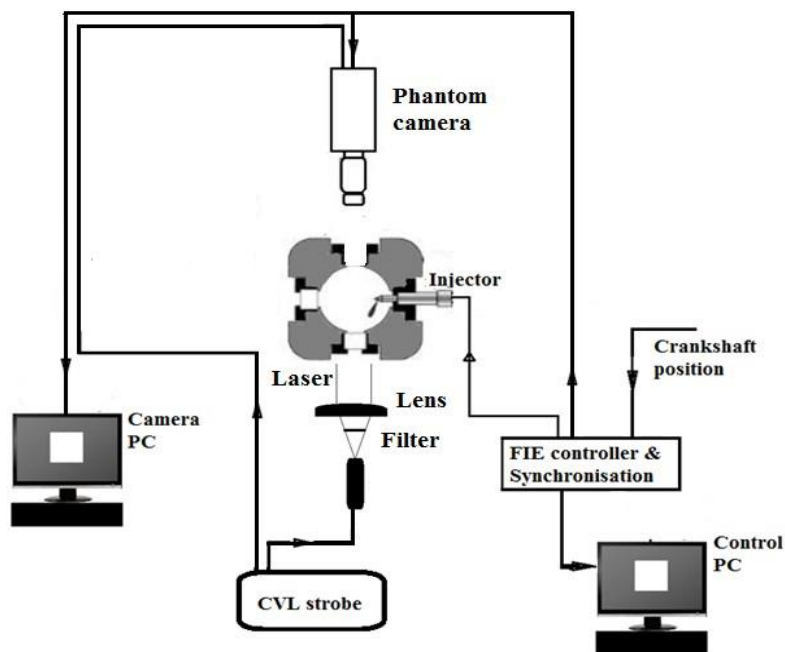


Figure 8: The schematic for the experimental set-up for the liquid vapour visualization. [34]

### *Fuel liquid spray visualization techniques*

The fuel liquid spray penetration values were measured using a Mie scattering technique, with the laser beam aligned to pass through the vertical plane of the fuel spray (Figure 7). With experiments involving injectors B, C and D, the laser light was collimated, at reduced intensity via neutral density filters. For injector A, experiments were not conducted with collimated light. Otherwise, the fuel liquid penetration tests were similar for all the injectors.

### *Fuel vapour spray visualization techniques*

The visualisation of the fuel vapour spray penetration tests for the present study were conducted using a shadowgraph technique (Figure 8). Though it was less sensitive than a Schlieren set-up, it was a simple and cheaper set-up because of the absence of a spatial Schlieren stop (e.g., knife edge) and a collecting (focussing) lens between the test chamber and the camera. Naturally, the spatial stop improves the sensitivity of a Schlieren layout; however the disturbing ambient gases (noise) in the combustion chamber become more apparent with the stop. The shadowgraph implemented in this work did not encounter this challenge; however the high resulting image intensity from the test chamber (reference frame) was well managed, in the absence of a focussing lens, by optimizing the camera focus. As a result, the camera lens was able to effectively clip-off the noise whilst projecting the reference frame on the camera CMOS chip.

### *Fuel vapour spray visualization technique sensitivity tests*

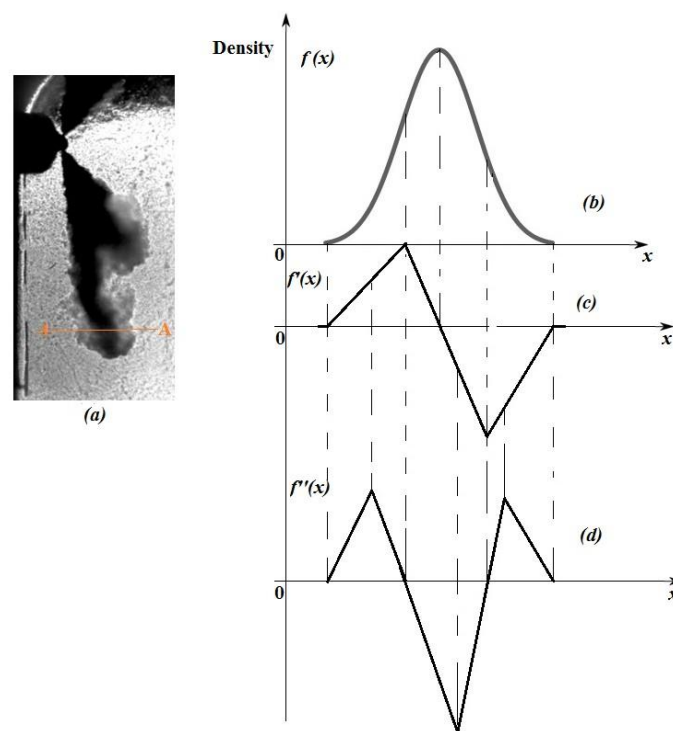


Figure 9: Details of the sensitivity tests for the shadowgraph technique used for the fuel vapour penetration tests. (a) shows the fuel vapour image, with cross-section A-A for the evaluation of the density changes. (b) to (d) show the variations in density across cross section A-A.

The sensitivity tests for the shadowgraph technique used for visualizing the fuel spray vapour penetration were carried out using the experimental configuration shown in Figure 8, with which the image in Figure 9(a) was acquired. A typical curve to illustrate the step change in density is constructed in Figure 9(b), as the parent function ( $f(x)$ ). The first ( $f'(x)$ ) and second ( $f''(x)$ ) derivatives of  $f(x)$ , shown in Figures 9(c) and 9(d) respectively, were determined by identifying the points of inflection: horizontal (maxima and minima points) and vertical. With these points, it was possible to determine the changes in sign of the derivatives (as shown in Figure 9(b) through to Figure 9(d)). Only Figure 9(d) significantly matched the A-A cross-section on the image in Figure 9(a). Across A-A, shades of white and grey are seen on either side of a continuous black band. The intensity plot at A-A shows the white and grey shades represented as peaks on either side of a steady darker profile, to confirm the similarity of the section and the profile in Figure 9(d).

#### *Uncertainty analysis*

The level of uncertainty in the measurements of the spray penetration values was determined by examining the accuracy of the measurement per pixel; this was determined as within  $\pm 1$  pixel. An example of the uncertainty values for Injector A is presented in Table 6.

Table 6: Percentage uncertainty values for the spray penetration measurements for Injector A under test point TP06 [see Table 7].

Time [ $\mu$ s]	Fuel spray penetration [mm]	% Uncertainty
431.99	3.5	2.38
456	7.09	1.18
479.99	8.87	0.94
504	10.87	0.77
551.99	15.04	0.55
576	17.79	0.47
600	20.51	0.41
623.98	22.36	0.37
647.99	23.47	0.36

The uncertainty in the fuel pressure measurements was presented in Table 4. The results for the spatial scale factors pre- and post-tests for all the injectors for liquid spray penetration tests were all within 0.3% of the pre-test mm/pixel values, indicating that the settings had not accidentally shifted during the experiments. Spray orientation checks showed the correctness of the positioning of the injectors at consistently right angle locations to the camera view. In summary, the analysis of the experimental uncertainties included all the sources of error and is quantified by the 95% confidence interval limits which are presented in the figures in the *Results and Discussion* sections.

## Test conditions used for the experiments

The test conditions for the fuel liquid and vapour spray penetration values were selected from the matrix presented in **Error! Reference source not found.** for investigations across the fuel injection pressure range. The fuel injection was timed at the TDC. The actual intake air temperature was determined by the intake manifold temperature (TMAN). The fuel spray parameters were quantified with respect to the time after the start of injection (ASOI) for every fuel spray plume.

Table 7: Test conditions used for the spray visualization, vapour and liquid penetration experiments.

Test point (TP)	Intake air temperature TMAN (°C)	Peak in-cylinder pressure ICP (bar)	Fuel pressure P (bar)	Injection quantity (mm <sup>3</sup> ) @ 38 °C
01	100	84	2000	65
02	100	84	1600	36.31
03	100	84	1400	36.71
04	100	84	1000	35.31
05	100	84	600	34.86
06	100	50	2000	45
07	100	50	1600	45
08	100	50	1400	45
09	100	50	1000	25
10	100	66	2000	65
11	100	66	1400	45
12	100	66	1000	45
13	100	79	1800	60
14	100	73	1600	50
15	100	40	600	20

## Image processing

After each test regime, the video images (at least 50) were read into an in-house MATLAB<sup>®</sup> based software and the post-processing was implemented by opening the images and subjecting them to enhancement as well as contour analysis (Figure 10). As the injectors used in this work were multi-hole, with corresponding number of spray plumes, a mask was applied to remove adjacent spray plumes and isolate a particular spray plume for processing. The spray contour obtained was analysed with respect to spray penetration by using the corresponding spatial resolution. The leading edge of the spray boundary is used to define the maximum liquid penetration (Figure 11).

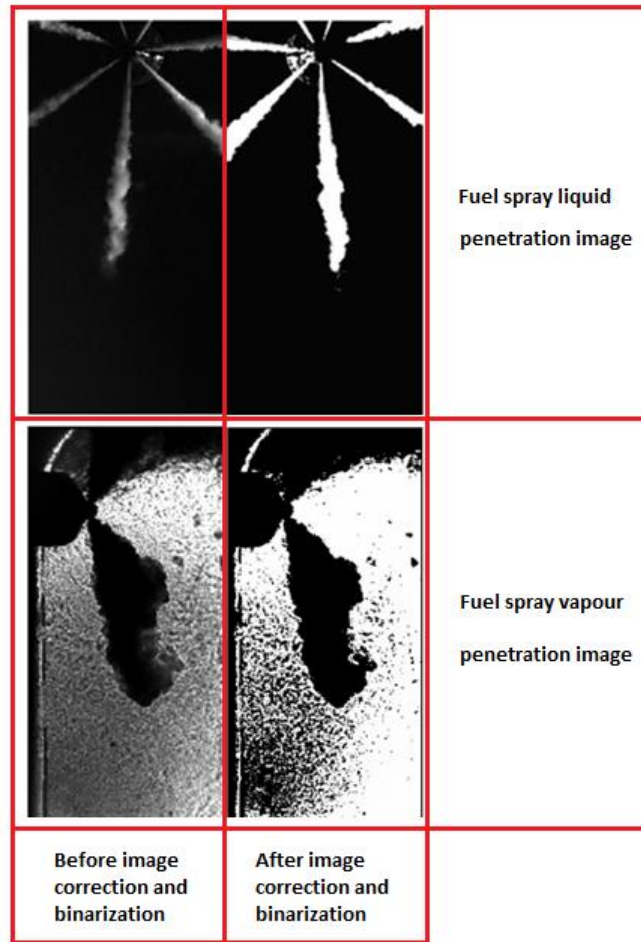


Figure 10: Fuel spray liquid and vapour images before and after correction and binarization.

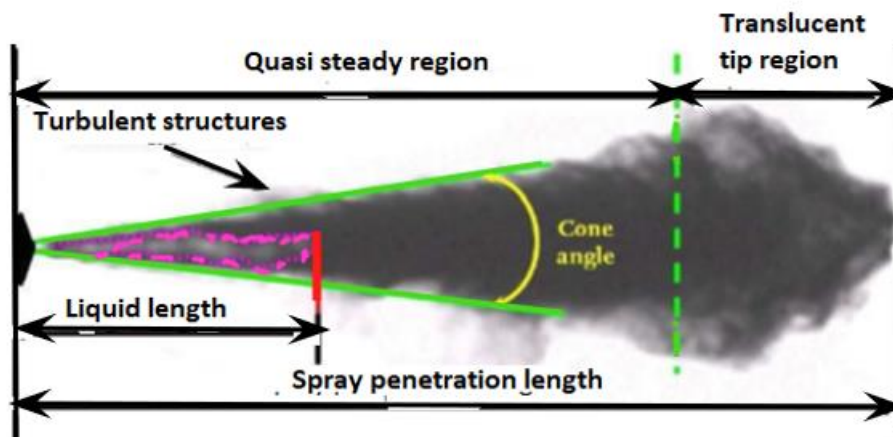


Figure 11: Definition of spray penetration. Adapted from the processed vapour spray image acquired with injector B at in-cylinder pressure of 40 bar, temperature of 100 °C, and injection pressure of 600 bar, test condition TP15 (Table 7).

## RESULTS AND DISCUSSION

### Spray images

Typical spray images from the four nozzle configurations are presented in Figure 12. They are snapshots at fuel injection time of  $1345\mu\text{s}$  at in-cylinder pressure of 40 bar and fuel injection pressure of 600 bar (condition TP15, Table 7). From these figures, it is difficult to derive qualitative differences from the different injectors but quantitative analyses in the following sections reveal the differences.

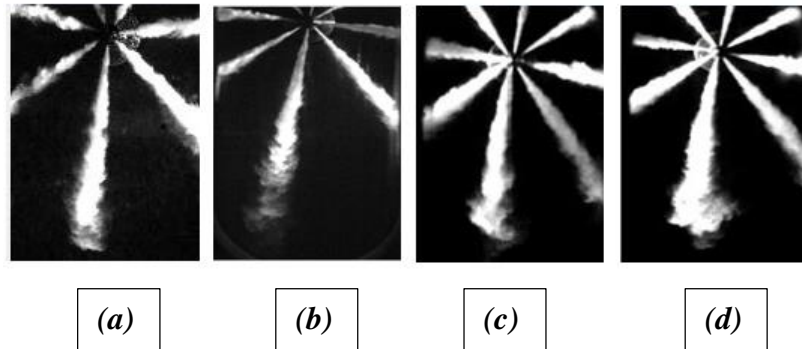


Figure 12: Images for liquid spray penetration at an injection time of  $1345\mu\text{s}$  at conditions of fuel injection pressure of 600 bar, and peak in-cylinder pressure of 40 bar (condition TP15 from Table 7) for, from (a) to (d), injectors A, B, C, and D, respectively.

### Influence of Fuel injection pressure values

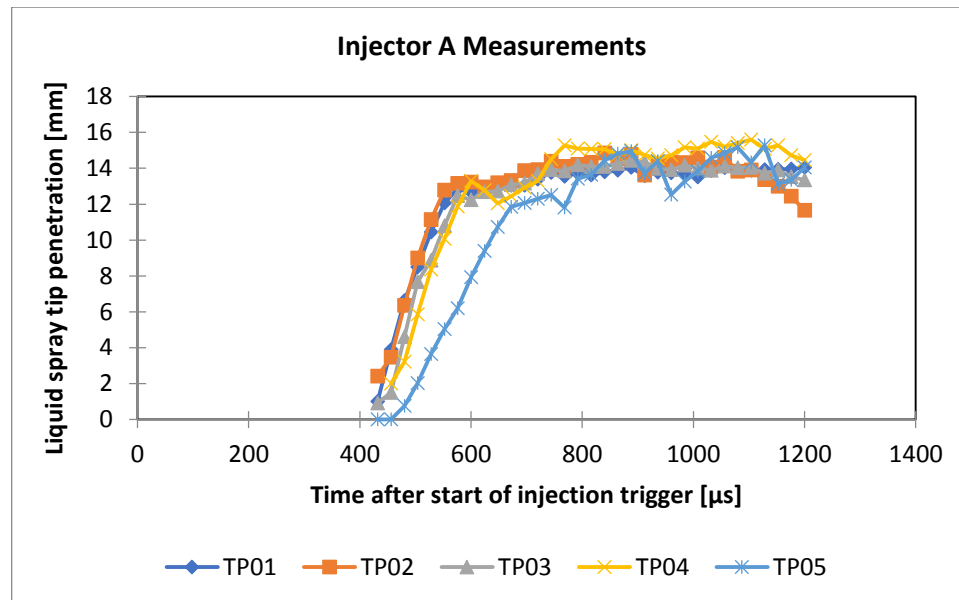


Figure 13: Fuel liquid spray penetration for injector A at 84 bar in-cylinder pressure at different fuel injection pressure values (TP1 to TP05, Table 7). Higher injection pressure values increase the spray penetration distances, however, the peak penetration values are close for all the conditions, and the differences decrease with increasing injection pressure values.

### *Spray liquid penetration*

The fuel spray liquid penetration tests indicate an initial phase of linear liquid penetration increase, with a slope of almost unity [3, 17] followed by a second phase of fluctuations around a fairly stable liquid penetration length [17], as can be seen from Figure 13. These fluctuations can occur due to some of the fuel liquid breaking off from the main fuel core due to the instability of the spray [17, 37]. The fuel injection pressure is especially significant at short time scales, as higher fuel injection pressure values lead to faster fuel liquid penetration due to higher initial fuel liquid momentum since

$$\dot{m}_f \propto (\Delta P)^{0.5} \quad (2)$$

Where  $\dot{m}_f$  is mass flow rate of fuel injected, (kg/s) and  $\Delta P$  is the pressure differential across the nozzle, (bar).

Thus, higher injection pressure values increase the fuel liquid core penetration rates, therefore leading to fully developed sprays in less time [17]. For example from Figure 13, the spray is fully developed at  $576\mu\text{s}$  for the 2000 bar fuel injection pressure case (TP01) and  $816\mu\text{s}$  for the 600 bar fuel injection pressure case (TP05). This is similar to the results for all the other injector (B, C, D) configurations (not shown here). However, the final fuel liquid penetration length is not greatly affected by the fuel injection pressure for all the cases tested, with the difference between the peak fuel liquid penetration length values between the 2000 bar and 600 bar fuel injection cases being less than 1.2 mm (see Figure 13). Also, the difference in the peak fuel liquid injection penetration values between each measured fuel injection pressure value and the preceding one (that is the peak value at 600 bar compared to at 1000 bar, peak value at 1000 bar compared to at 1400 bar, etc.) begins to narrow as the fuel injection pressure increases. This is understandable as from [16]

$$S \propto (\Delta P)^{0.25} \quad (3)$$

Where  $S$  is the fuel spray tip penetration, (mm) and  $\Delta P$  is the pressure differential across the nozzle, (bar).

Also, pressure loss becomes more significant at higher fuel injection pressure values because of the injector body and nozzle throttle [16]. It was noted that there was a longer time delay between the injection signal and the first recording of the fuel exit from the nozzle for all the tests conducted for injector A at 84 bar/600 bar (TP05) and for injector B at 50 bar/1000 bar (TP09), compared to the other test points. See Figures 13 and 14, for instance. However, this behaviour has previously been noted by others (see [16], for example), and do not affect the conclusions from the present test results.

### *Spray vapour penetration*

The fuel spray vapour penetration results indicate higher values than the fuel spray liquid penetration for corresponding conditions. Whereas fuel liquid penetration reaches a maximum soon after the start of injection (Figure 13, for example), the fuel vapour penetration (Figure 14) continues to rise with time after the start of the injection trigger until it reaches a maximum (also observed by [8, 17, 13]). The liquid phase momentum exchange between the fuel droplets and the carrier gas results in the gas motion and this is responsible for the fuel vapour transportation. This phenomenon is

reinforced by the fact that even for low carrier gas density values, higher injection pressure values result in increased fuel vapour penetration, indicating higher fuel liquid phase momentum [8]. Higher fuel injection pressure values enhance the fuel vapour penetration; the greater momentum impacted onto the fuel liquid results in the production of a higher number of small sized droplets and also in the faster evaporation of the droplets.

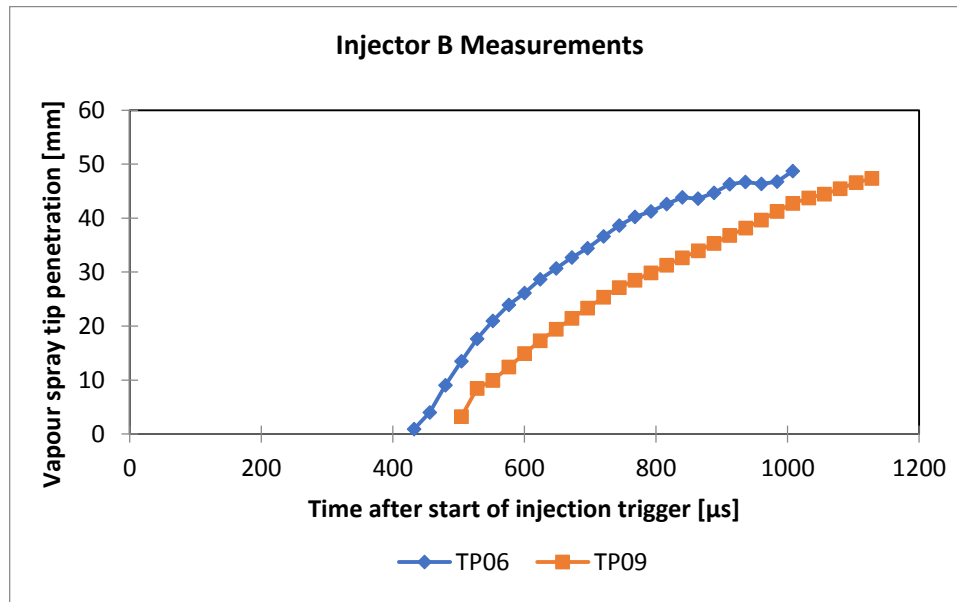


Figure 14: Fuel spray vapour penetration for injector B at 50 bar in-cylinder pressure at different fuel injection pressure values. These continue to propagate and rise with time after the start of injection.

### Influence of In-cylinder pressure values

#### *Spray liquid and vapour penetration*

The results for the effects of the in-cylinder pressure values on the fuel spray liquid and vapour penetration values are presented in Figures 15 and 16. These follow the same trend as the influence of the fuel injection pressure values in the previous section, albeit in reverse. The in-cylinder pressure presents a resistance to the fuel spray liquid and vapour penetration [36], therefore an increase in the value reduces the fuel spray liquid and vapour penetration values.

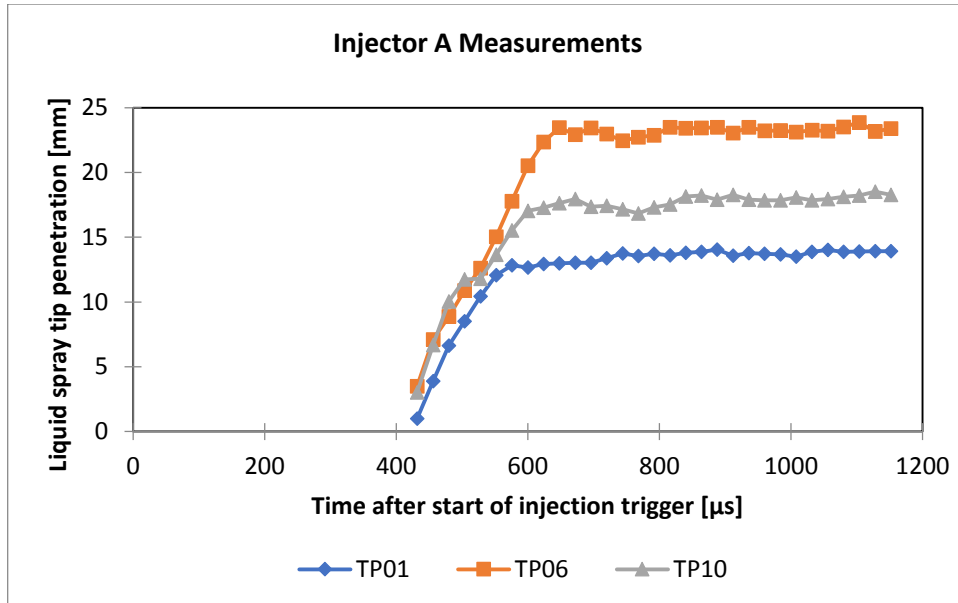


Figure 15: Fuel spray liquid penetration for injector A at 2000 bar injection pressure at different in-cylinder pressure values. An increase in ICP value reduces the spray penetration.

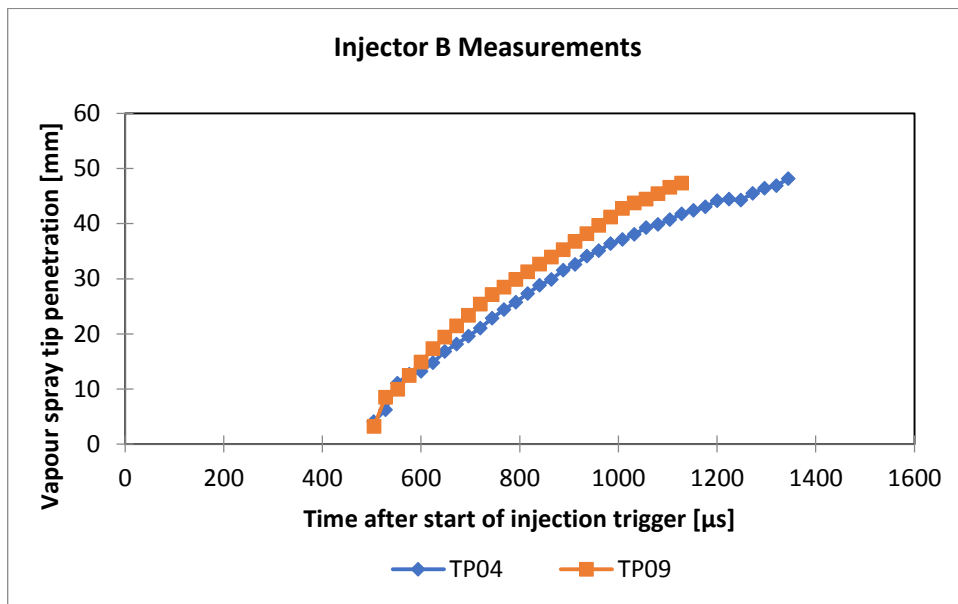


Figure 16: Fuel spray vapour penetration for injector B at 1000 bar injection pressure at different in-cylinder pressure values. An increase in ICP value reduces the spray penetration.

1  
2  
3  
4  
5  
6  
7  
8  
9  
10  
11  
12  
13  
14  
15  
16  
17  
18  
19  
20  
21  
22  
23  
24  
25  
26  
27  
28  
29  
30  
31  
32  
33  
34  
35  
36  
37  
38  
39  
40  
41  
42  
43  
44  
45  
46  
47  
48  
49  
50  
51  
52  
53  
54  
55  
56  
57  
58  
59  
60  
61  
62  
63  
64  
65

## Influence of Injector nozzle configuration

### Spray liquid and vapour penetration

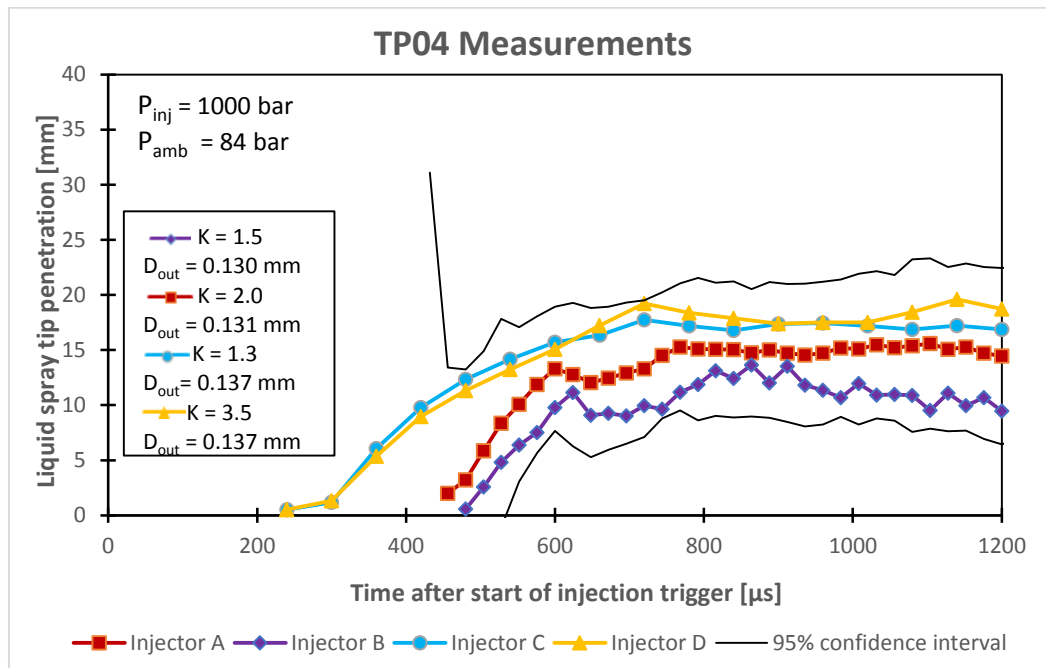


Figure 17: Fuel spray liquid penetration; the effect of injector nozzle type at TP04 conditions [Table 7]. The larger sized nozzles present longer spray penetration.

The effects of the injector nozzle configuration on the fuel spray liquid and vapour penetration values are presented using Figures 17 to 26. The injectors are closely related in two groups; injectors A & B, and injectors C & D. The only difference between injectors C & D is their conicity (see equation (1) and Table (5)). Figure 17 shows that the group of injectors with the larger diameter nozzles (injectors C & D – 0.137 mm) present higher fuel spray liquid penetration values compared to those with smaller sized diameter nozzles (injector A (0.131 mm) & injector B (0.130 mm)). Larger diameter nozzles allow larger fuel mass rate values to be injected (see Table 5), increasing the fuel liquid momentum and, hence, the fuel spray liquid penetration [38]. The rest of the section on the effect of the injector configuration will be restricted to results from injectors C and D as the conicity value is their only differentiator.

Injectors C and D both have positive  $k$ -factor values (Table 5; Figures 5 and 6), thus the orifice diameter decreases towards the nozzle exit (equation 1). Injectors with negative and zero  $k$ -factor values might suffer from cavitation, as the fuel flow pressure is more likely to fall below the vapour pressure of the fuel liquid leading to the formation of bubbles. If the cavitation is excessively strong the nozzle might be damaged. However, for nozzles with positive  $k$ -factor values, cavitation and turbulence values inside the orifice are reduced, slowing down primary breakup, larger droplets are produced as a consequence, leading to increased spray penetration as they are carried further downstream. Other scholars have also observed these trends [39, 40]. From Figure 17, the maximum fuel spray liquid penetration for Injector D ( $k$ -factor = 3.5) is further than that of injector C ( $k$ -factor = 1.3), however this effect is not significant, as has been observed elsewhere [40].

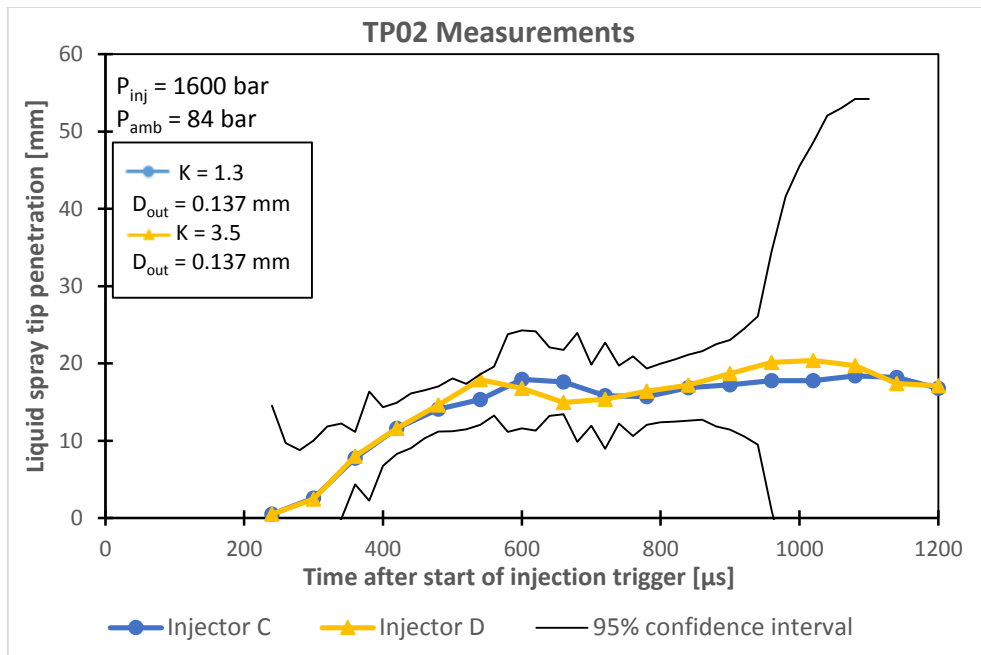


Figure 18: Fuel spray liquid penetration; the effect of injector nozzle type at TP02 conditions [Table 7]. The injector with the larger  $k$ -factor has an insignificantly longer spray penetration.

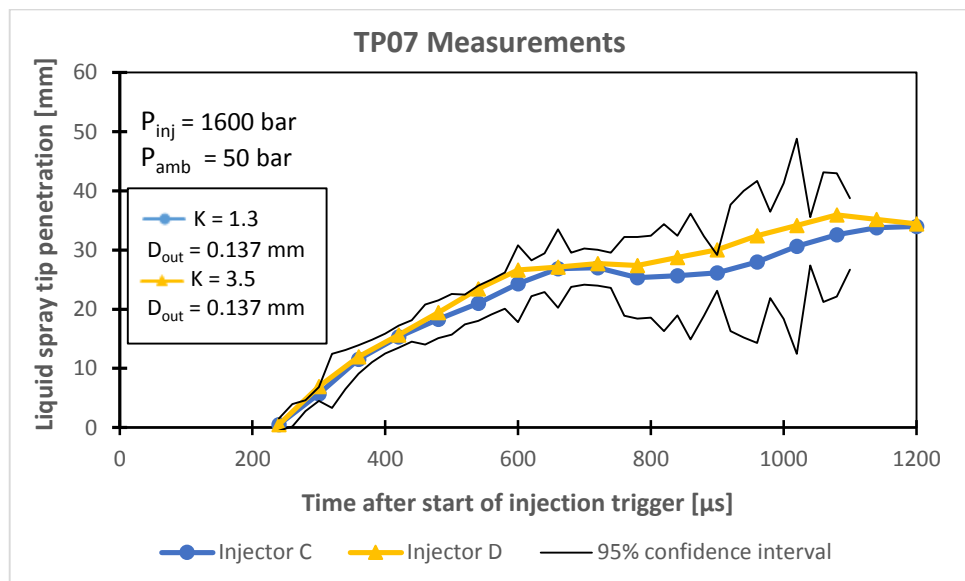


Figure 19: Fuel spray liquid penetration; the effect of injector nozzle type at TP07 conditions [Table 7]. The injector with the larger  $k$ -factor has an insignificantly longer spray penetration.

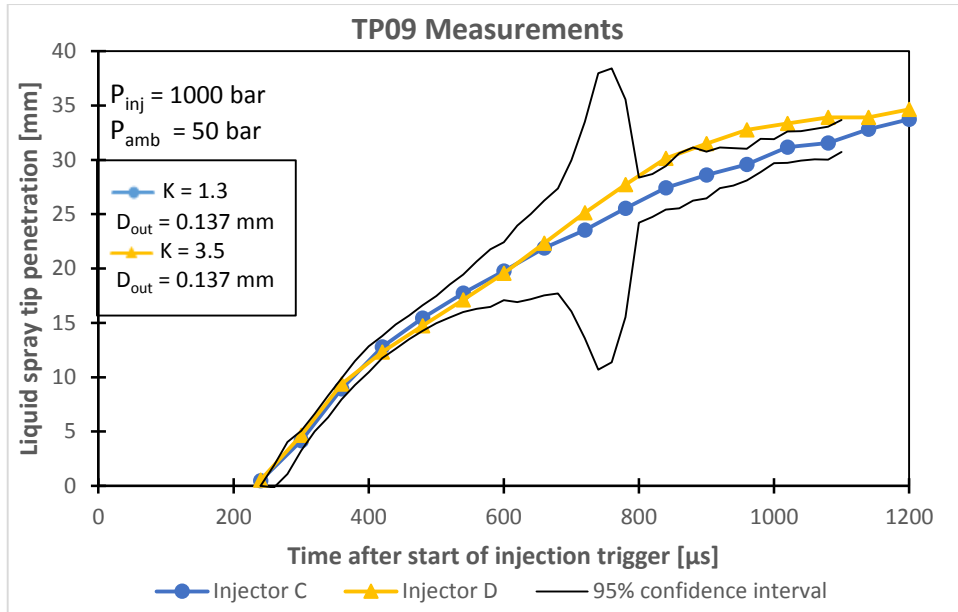


Figure 20: Fuel spray liquid penetration; the effect of injector nozzle type at TP09 conditions [Table 7]. The injector with the larger  $k$ -factor has an insignificantly longer spray penetration.

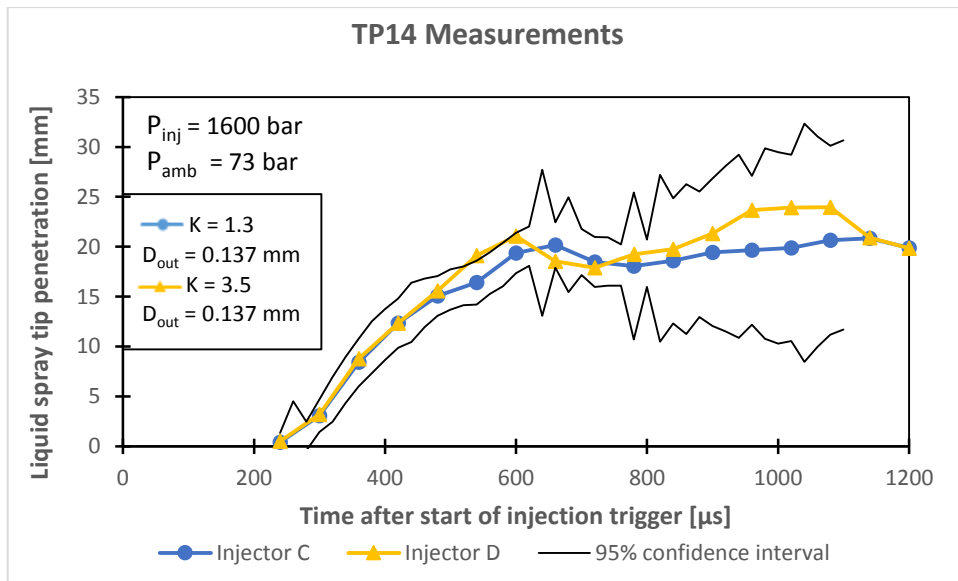


Figure 21: Fuel spray liquid penetration; the effect of injector nozzle type at TP14 conditions [Table 7]. The injector with the larger  $k$ -factor has an insignificantly longer spray penetration.

1  
2  
3  
4  
5  
6  
7  
8  
9  
10  
11  
12  
13  
14  
15  
16  
17  
18  
19  
20  
21  
22  
23  
24  
25  
26  
27  
28  
29  
30  
31  
32  
33  
34  
35  
36  
37  
38  
39  
40  
41  
42  
43  
44  
45  
46  
47  
48  
49  
50  
51  
52  
53  
54  
55  
56  
57  
58  
59  
60  
61  
62  
63  
64  
65

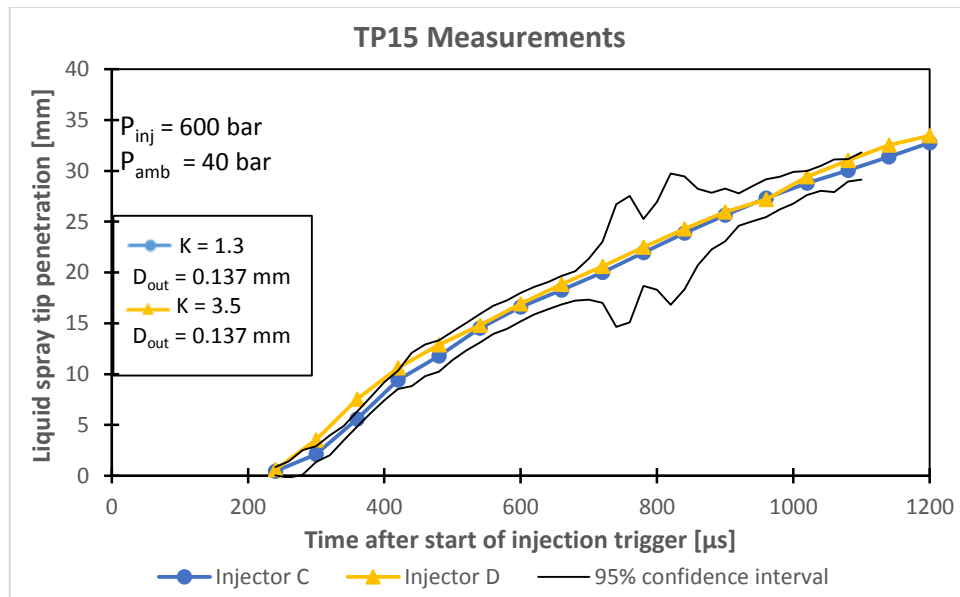


Figure 22: Fuel spray liquid penetration; the effect of injector nozzle type at TP15 conditions [Table 7]. The injector with the larger  $k$ -factor has an insignificantly longer spray penetration.

This trend continues for the other test conditions, as shown in Figures 18 to 22. The fuel spray liquid penetration values for the injector with a higher conicity value (Injector D;  $k$ -factor = 3.5) is further than those for the injector with a lower conicity value (injector C;  $k$ -factor = 1.3), but the differences are within the experimental error and not significant.

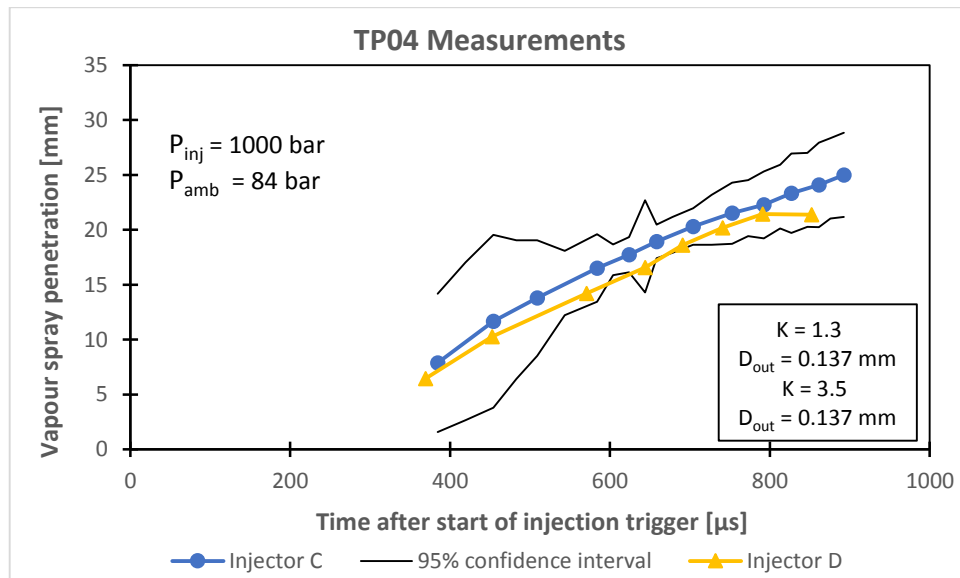


Figure 23: Fuel spray vapour penetration; the effect of injector nozzle type at TP04 conditions [Table 7]. The injector with the smaller  $k$ -factor has an insignificantly longer spray penetration.

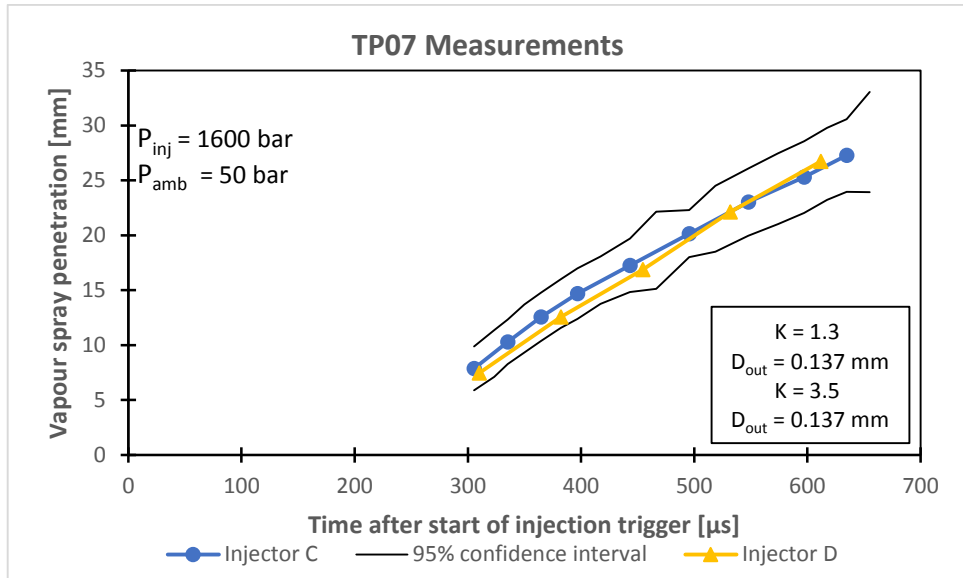


Figure 24: Fuel spray vapour penetration; the effect of injector nozzle type at TP07 conditions [Table 7]. The injector with the smaller  $k$ -factor has an insignificantly longer spray penetration.

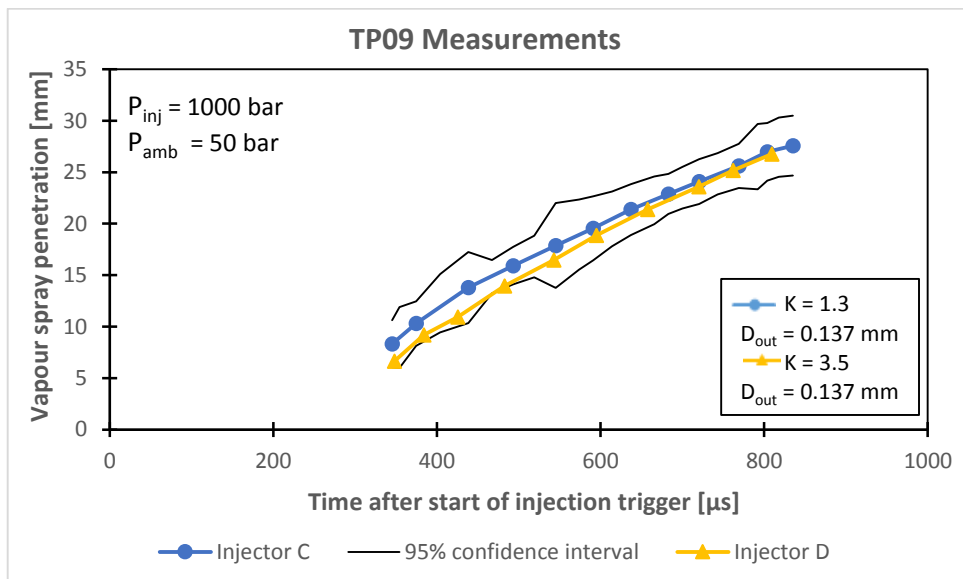


Figure 25: Fuel spray vapour penetration; the effect of injector nozzle type at TP09 conditions [Table 7]. The injector with the smaller  $k$ -factor has an insignificantly longer spray penetration.

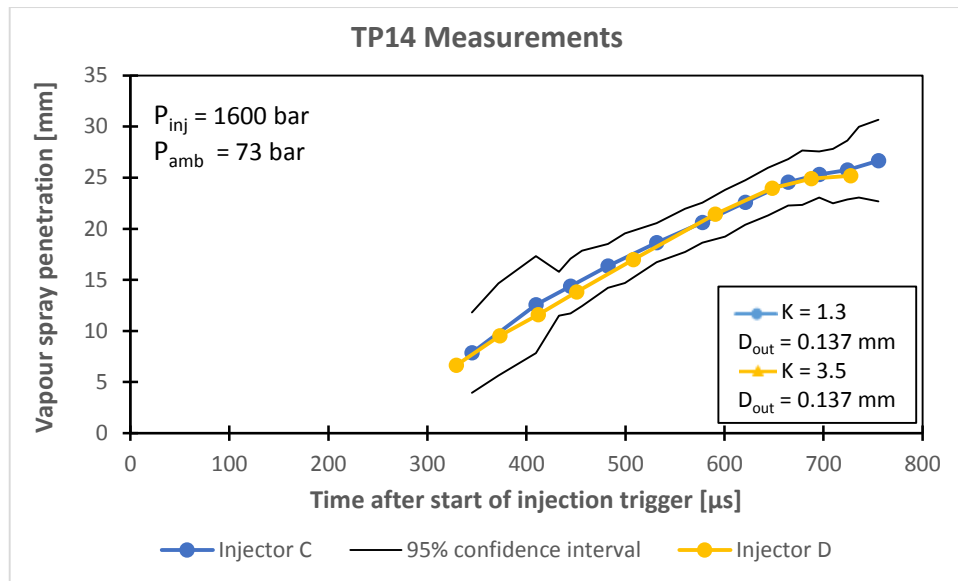


Figure 26: Fuel spray vapour penetration; the effect of injector nozzle type at TP14 conditions [Table 7]. The injector with the smaller  $k$ -factor has an insignificantly longer spray penetration.

The effect of conicity of the injectors on the fuel spray vapour penetration is presented in Figures 23 to 26. Contrary to the fuel spray liquid penetration results, the *peak* fuel spray vapour penetration values for the injector with a higher conicity value (Injector D;  $k$ -factor = 3.5) are shorter than those for the injector with a lower conicity value (injector C;  $k$ -factor = 1.3), but the differences are within the experimental error and not significant. Therefore, the insignificant differences are similar to those from the fuel spray liquid penetration studies presented in Figures 17 to 22. Such studies are uncommon in literature; however, an earlier study [34] ascribed the longer fuel spray vapour penetration values usually observed against the fuel spray liquid penetration values at corresponding fuel injection pressure values to the effect of the  $k$ -factor. In the present studies, for instance, comparing Figure 21 with Figure 26, the fuel spray vapour penetration is  $\sim 40\%$  further at  $720\mu\text{s}$  after the start of injection compared to the fuel spray liquid penetration values for both injectors C and D measured at the same time. But from the results presented here, this phenomenon is more likely as a consequence of the continued propagation of the vapour phase beyond the liquid phase as has been noted in *spray vapour penetration* section. The liquid phase momentum exchange between the fuel droplets and the carrier gas results in the gas motion that accounts for the fuel vapour transportation and the fuel vapour cloud alongside the liquid core continues beyond the peak liquid length [17]. Carrying out further studies at fuel injection pressures of above 3300 bar might better elucidate the effects of the different nozzle configuration on the liquid/spray vapour penetration.

## Practical implications

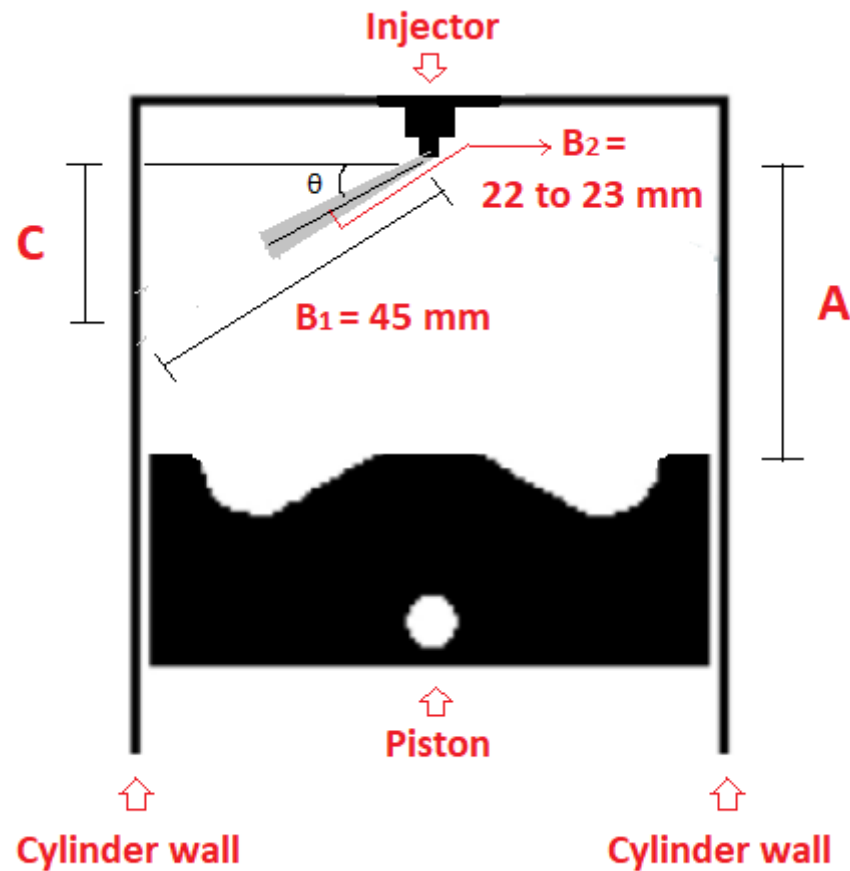


Figure 27: Schematic of a piston inside a typical 2.0 L compression ignition engine [17]. Adapted from [41]; not to scale. **A**: the distance between the injector nozzle tip and the piston bowl surface at the top dead centre. **B**: the distance between the injector nozzle tip and the cylinder wall liner surface, along the centre of the spray axis; **B**<sub>1</sub> = distance using the injector system in [17], **B**<sub>2</sub> = distances using the injectors in the current study for conditions TP06 to TP09 from Table 7. **C**: the vertical distance between the injector nozzle tip and the point at which spray hits the cylinder wall liner surface. For the conditions TP06 to TP09 from Table 7 presented in this study, **A** > **C**. Therefore, wall liner surface and piston bowl surface, wetting is unlikely to be of concern at these conditions.

A 2.0L compression ignition engine, with an absolute intake pressure range of 2 to 2.5 bar and a compression ratio range of 17 to 18.5:1, an injector nozzle to cylinder liner surface distance of about 45 mm (for a full cone angle of 11°), and an injector to piston bowl surface distance, at the top dead centre, of 25 mm [17], has been used to illustrate the practical applications of the results from this study; the reader can relate this to any other engine of known specifications. From Figure 27, these tests enable researchers and designers to evaluate the consequences of fuel spray liquid and vapour penetration values; if these values are greater than the distance 'B' this could lead to wall wetting, increased wall wear, reduced combustion efficiency and higher emissions due to unburned fuel, for example. If distance 'A' is smaller than distance 'C' then the injection timing has to be synchronised to control the effects of similar consequences related to the fuel spray liquid and or vapour impacting on the piston bowl surface.

1 Figure 27 shows that, for the fuel spray liquid penetration values observed for  
2 conditions TP06 to TP09 (Table 7), the spray liquid will not hit the cylinder liner walls.  
3 This is a feature of using rapid cycling machines, which are fitted with production  
4 engine piston designs allowing for the examination of practical operating conditions for  
5 internal combustion engines.  
6

## 7 **Conclusions**

8  
9 As electric propulsion, and indeed, alternative green propulsion systems might not be  
10 available in many regions worldwide or applicable to many uses (off-road vehicles, off-  
11 grid generator sets, and marine engines, for example) for some time, work on improving  
12 the efficiency of internal combustion engines must continue so as to reduce the  
13 emissions due to their use. Rapid Cycling Machines allow for the characterisation of  
14 the performance of internal combustion engines under realistic engine operating  
15 conditions using regular piston designs. In this study the influence of the injector  
16 configuration, in-cylinder pressure and injection pressure conditions on the fuel spray  
17 vapour and liquid penetration were assessed. The injection pressure conditions were at  
18 25% higher than values than have been typically reported for rapid cycling machines,  
19 thus more representative of current engine operating conditions.  
20  
21  
22

23 Four injectors of different  $k$ -factor configurations, ranging from 1.5 to 3.5, were used.  
24 Fifteen different operating conditions for combinations of fuel injection pressure  
25 values, ranging from 600 to 2000 bar, and in-cylinder pressure values, ranging from 40  
26 to 84 bar, were evaluated. Visual inspections of the spray propagation from the various  
27 nozzle configurations present no discernible differences. The results indicate that the  
28 fuel spray liquid penetration rates increased with increases in the fuel injection pressure  
29 values, but the final fuel liquid penetration length values were not remarkably different,  
30 being less than 1.2 mm between the 2000 bar and 600 bar fuel injection final fuel liquid  
31 penetration values. The fuel spray vapour penetration results indicate longer values  
32 compared to the fuel spray liquid penetration, as the fuel vapour propagates further and  
33 is almost linear with time, with higher injection pressure values generating longer fuel  
34 spray vapour lengths. The in-cylinder pressure acts as a resistance to the fuel spray  
35 propagation and increasing the value has a constraining effect on fuel spray liquid and  
36 vapour penetration values. The liquid penetration values increase with increasing  $k$ -  
37 factor values for the injector nozzles, and the reverse is the case for the vapour  
38 penetration values but these effects are not significant, and well within the experimental  
39 error values; the effects of the in-cylinder and fuel injection pressure are more  
40 dominant. However, further exploring the effects of the injector configuration using  
41 rapid cycling machines at injector pressure values of up to 3300 bar presently possible  
42 using combustion “bombs” might reveal changes that are more significant. The results  
43 presented here using the rapid cycling machine are important and an example of the  
44 results applied to a standard 2.0L diesel engine is presented. This is because fuel spray  
45 impingement on the cylinder liner walls and piston bowl can contribute to higher  
46 emissions due to the increase in unburned fuel liquid as a consequence of wetting of the  
47 walls; researchers and designers are keen to minimize these.  
48  
49  
50  
51  
52  
53  
54  
55  
56  
57  
58  
59  
60  
61  
62  
63  
64  
65

## References

1. Ewing, J. and Davenport, C., 2015. Volkswagen to Stop Sales of Diesel Cars Involved in Recall. *The New York Times*.  
<https://www.nytimes.com/2015/09/21/business/international/volkswagen-chief-apologizes-for-breach-of-trust-after-recall.html>. Accessed June 4, 2019.
2. Regulation (EC) No 715/2007 of the European Parliament and of the Council of 20 June 2007. *Official Journal of the European Union*. <https://eur-lex.europa.eu/legal-content/EN/TXT/?qid=1559223983682&uri=CELEX:32007R0715>. Accessed June 4, 2019.
3. Lefebvre, A.H. and McDonell, V.G., 2017. *Atomization and Sprays*. CRC Press, Boca Raton, USA.
4. Baert, R.S., Frijters, P.J., Somers, B., Luijten, C.C. and de Boer, W., 2009. *Design and operation of a high pressure, high temperature cell for HD diesel spray diagnostics: guidelines and results* (No. 2009-01-0649). SAE Technical Paper.
5. Winklhofer, E. and Hopfner, W., 2013. Optical single cylinder engines in engine research and development. *Silniki Spalinowe*, 52, pp.71-78.
6. Espey, C. and Dec, J.E., 1993. *Diesel engine combustion studies in a newly designed optical-access engine using high-speed visualization and 2-D laser imaging* (No. 930971). SAE Technical Paper.
7. Sung, C.J. and Curran, H.J., 2014. Using rapid compression machines for chemical kinetics studies. *Progress in Energy and Combustion Science*, 44, pp.1-18.
8. Naber, J.D. and Siebers, D.L., 1996. *Effects of gas density and vaporization on penetration and dispersion of diesel sprays*. (No. 960034). SAE Technical Paper.
9. Pickett, L.M., Genzale, C.L., Bruneaux, G., Malbec, L.M., Hermant, L., Christiansen, C. and Schramm, J., 2010. Comparison of diesel spray combustion in different high-temperature, high-pressure facilities. *SAE International Journal of Engines*, 3(2), pp.156-181.
10. Bardi, M., Payri, R., Malbec, L.M.C., Bruneaux, G., Pickett, L.M., Manin, J., Bazyn, T. and Genzale, C.L., 2012. Engine combustion network: comparison of spray development, vaporization, and combustion in different combustion vessels. *Atomization and Sprays*, 22(10).
11. Kennaird, D., Crua, C., Heikal, M., Morgan, R., Bar, F. and Sapsford, S., 2000, November. A new high-pressure diesel spray research facility. In *IMEchE Conference Transactions* (Vol. 8, pp. 179-188). Professional Engineering Publishing; 1998.
12. Palanisamy, M., Lorch, J., Truemner, R.J. and Baldwin, B., 2015. Combustion characteristics of a 3000 bar diesel fuel system on a single cylinder research engine. *SAE International Journal of Commercial Vehicles*, 8(2015-01-2798), pp.479-490.
13. Johnson, J., Naber, J., Lee, S.Y., Hunter, G., Truemner, R. and Harcombe, T., 2013. *Correlations of non-vaporizing spray penetration for 3000 bar diesel spray injection* (No. 2013-24-0033). SAE Technical Paper.

14. Boccardo, G., Millo, F., Piano, A., Arnone, L., Manelli, S., Fagg, S., Gatti, P., Herrmann, O.E., Queck, D. and Weber, J., 2019. Experimental investigation on a 3000 bar fuel injection system for a SCR-free non-road diesel engine. *Fuel*, 243, pp.342-351.
15. Wloka, J.A., Pflaum, S. and Wachtmeister, G., 2010. Potential and challenges of a 3000 bar common-rail injection system considering engine behavior and emission level. *SAE International Journal of Engines*, 3(1), pp.801-813.
16. Morgan, R., Gold, M., Wray, J. and Whelan, S., 2001. *A study of the formation and break-up of a Diesel spray for HSDI Diesel engine combustion systems*. In: The Fifth International Symposium on Diagnostics and Modeling of Combustion in Internal Combustion Engines (COMODIA). July 1 – 4, 2001, Nagoya, Japan.
17. Laguitton, O., Gold, M.R., Kennaird, D.A., Crua, C., Lacoste, J. and Heikal, M., 2002. *Spray development and combustion characteristics for common rail diesel injection systems*. In: IMechE Conference on Fuel Injection Systems, 26-27 Nov 2002, London, UK.
18. Lacoste, J., Crua, C., Heikal, M., Kennaird, D. and Gold, M., 2003. *PDA characterisation of dense diesel sprays using a common-rail injection system*. (No. 2003-01-3085) SAE Technical Paper.
19. Zegers, R.P.C., Luijten, C.C.M., Dam, N.J. and De Goey, L.P.H., 2012. Pre- and post-injection flow characterization in a heavy-duty diesel engine using high-speed PIV. *Experiments in fluids*, 53(3), pp.731-746.
20. Morgan, R., Banks, A., Auld, A. and Heikal, M., 2015. *The Benefits of High Injection Pressure on Future Heavy Duty Engine Performance* (No. 2015-24-2441). SAE Technical Paper.
21. Wickman, D.D., Tanin, K.V., Senecal, P.K., Reitz, R.D., Gebert, K., Barkhimer, R.L. and Beck, N.J., 2000. *Methods and Results from the Development of a 2600 Bar Diesel Fuel Injection System* (No. 2000-01-0947). SAE Technical Paper.
22. Arcoumanis, C., Whitelaw, J.H., Hentschel, W. and Schindler, K.P., 1994. Flow and combustion in a transparent 1.9 litre direct injection Diesel engine. *Proceedings of the Institution of Mechanical Engineers, Part D: Journal of Automobile Engineering*, 208(3), pp.191-205.
23. Musculus, M.P., 2006. *Multiple simultaneous optical diagnostic imaging of early-injection low-temperature combustion in a heavy-duty diesel engine* (No. 2006-01-0079). SAE Technical Paper.
24. Dembinski, H., 2014. *In-cylinder Flow Characterisation of Heavy Duty Diesel Engines Using Combustion Image Velocimetry*. Doctoral dissertation, KTH Royal Institute of Technology, Stockholm, Sweden.
25. Mueller, C.J., Martin, G.C., Briggs, T.E. and Duffy, K.P., 2004. *An experimental investigation of in-cylinder processes under dual-injection conditions in a DI diesel engine*. (No. 2004-01-1843). SAE Technical Paper.
26. Fuyuto, T., Matsumoto, T., Hattori, Y., Kugimoto, K., Fujikawa, T., Akihama, K. and Ito, H., 2012. A new generation of optically accessible single-cylinder engines for high-speed and high-load combustion analysis. *SAE International Journal of Fuels and Lubricants*, 5(1), pp.307-315.
27. Jia, T.M., Yu, Y.S. and Li, G.X., 2017. Experimental investigation of effects of super high injection pressure on diesel spray and induced shock waves characteristics. *Experimental Thermal and Fluid Science*, 85, pp.399-408.

- 1 28. Nishida, K., Zhu, J., Leng, X. and He, Z., 2017. Effects of micro-hole nozzle  
2 and ultra-high injection pressure on air entrainment, liquid penetration, flame  
3 lift-off and soot formation of diesel spray flame. *International Journal of*  
4 *Engine Research*, 18(1-2), pp.51-65.
- 5 29. Njere, D.O., 2015. *Optical Characterisation of high pressure diesel fuel*  
6 *injectors*. MPhil Thesis, University of Brighton, UK.
- 7 30. Faure, M.A., Sadler, M., Oversby, K.K., Stokes, J., Begg, S.M., Pommier, L.S.  
8 and Heikal, M.R., 1998. *Application of LDA and PIV techniques to the*  
9 *validation of a CFD model of a direct injection gasoline engine*. (No. 982705)  
10 SAE Technical Paper.
- 11 31. Payri, R., Salvador, F.J., Gimeno, J. and De la Morena, J., 2011. Influence of  
12 injector technology on injection and combustion development–Part 1:  
13 Hydraulic characterization. *Applied Energy*, 88(4), pp.1068-1074.
- 14 32. Roth, H., Gavaises, M. and Arcoumanis, C., 2002. *Cavitation initiation, its*  
15 *development and link with flow turbulence in diesel injector nozzles*. (No.  
16 2002-01-0214) SAE Technical Paper.
- 17 33. Brusiani, F., Falfari, S. and Pelloni, P., 2014. Influence of the Diesel injector  
18 hole geometry on the flow conditions emerging from the nozzle. *Energy*  
19 *Procedia*, 45, pp.749-758.
- 20 34. Njere, D. and Emekwuru, N., 2017. Fuel spray vapour distribution for high-  
21 pressure diesel fuel spray cases for different injector nozzle geometries. In  
22 *ILASS Europe. 28th European Conference on Liquid Atomization and Spray*  
23 *Systems* (pp. 192-199). Editorial Universitat Politècnica de València.
- 24 35. Njere, D. and Emekwuru, N., 2018, Analysis of spray penetration models  
25 applied to high pressure diesel spray cases for different injector nozzle  
26 geometries. In *ICLASS 2018. 14<sup>th</sup> Triennial International Conference on*  
27 *Liquid Atomization and Spray Systems*. Chicago, USA.
- 28 36. Heywood, J.B., 2018. *Internal Combustion Engine Fundamentals*. McGraw-  
29 Hill Education. New York, USA.
- 30 37. Kennaird, D.A., Crua, C., Lacoste, J., Heikal, M.R., Gold, M.R. and Jackson,  
31 N.S., 2002. *In-cylinder penetration and break-up of diesel sprays using a*  
32 *common-rail injection system* (No. 2002-01-1626). SAE Technical Paper.
- 33 38. Emekwuru, N.G., 2012, Progress with the analysis of dimethyl ether sprays  
34 with a moments spray model. In *ICLASS-2012, Proceedings of the 12th*  
35 *Triennial International Conference on Liquid Atomization and Spray Systems*.  
36 Heidelberg, Germany.
- 37 39. Payri, F., Payri, R., Salvador, F.J. and Gimeno, J., 2007. *Influence of nozzle*  
38 *geometry on spray characteristics in non-evaporative and evaporative*  
39 *conditions* (No. 2007-24-0023). SAE Technical Paper.
- 40 40. Tang, C., Feng, Z., Zhan, C. and Huang, Z., 2017. Experimental study on the  
41 effect of injector nozzle K factor on the spray characteristics in a constant  
42 volume chamber: Near nozzle spray initiation, the macroscopic and the droplet  
43 statistics. *Fuel*, 202, pp.583-594.
- 44 41. Boot, M., Rijk, E., Luijten, C., Somers, B. and Albrecht, B., 2010. *Spray*  
45 *impingement in the early direct injection premixed charge compression*  
46 *ignition regime* (No. 2010-01-1501). SAE Technical Paper.

## NOMENCLATURE

1		
2		
3		
4		
5	ASOI	Time after the start of injection, ( $\mu\text{s}$ )
6	CO	Carbon Monoxide
7	CR	Compression ratio
8	CRS	Common-rail system
9	CVL	Copper-vapour laser
10	DC	Direct current
11	$D_{\text{inlet}}$	Inlet orifice diameter, ( $\mu\text{m}$ )
12	$D_{\text{outlet}}$	Outlet orifice diameter, ( $\mu\text{m}$ )
13	EGR	Exhaust Gas Recirculation
14	HC	Hydrocarbons
15	HP	High pressure
16	ICP	In-cylinder pressure, (bar)
17	$k$	$k$ -factor
18	$\dot{m}_f$	Mass flow rate of fuel injected, (kg/s)
19	$\text{NO}_x$	Nitrogen Oxide
20	OARE	Optically Accessed Research Engines
21	PM	Particulate Matter
22	PN	Particle Number
23	$S$	Fuel spray tip penetration, (mm)
24	TDC	Top dead centre
25	TMAN	Intake manifold temperature, ( $^{\circ}\text{C}$ )
26	VCO	Valve covering orifice
27	$\Delta P$	Pressure differential across the nozzle, (bar)
28		
29		
30		
31		
32		
33		
34		
35		
36		
37		
38		
39		
40		
41		
42		
43		
44		
45		
46		
47		
48		
49		
50		
51		
52		
53		
54		
55		
56		
57		
58		
59		
60		
61		
62		
63		
64		
65		